Slow electrons impinging on dielectric solids. II. Implantation profiles, electron mobility, and recombination processes

Antonio Miotello
INFM and Dipartimento di Fisica dell'Università di Trento, I-38050 Povo, Trento, Italy

Maurizio Dapor
INFM and Centro Materiali e Biofisica Medica, Istituto Trentino di Cultura, I-38050 Povo, Trento, Italy
(Received 2 December 1996)

When an insulator is subject to electron irradiation, a fraction of electrons is absorbed while the rest is backscattered. The injected electrons cannot be definitely trapped but they must instead recombine with positive charges left near the irradiated surface when secondary electrons are emitted; this is justified on the basis that dielectric breakdown is not observed during specific experiments of electron irradiation of insulators. The dynamics of the absorbed electrons depend on a number of parameters: the number of trapped electrons, the charge-space distribution, the mobility, and the number of secondary electrons emitted from the region near the surface of the dielectric. The time evolution of the surface electric has been studied by integration of the continutity equation for the relevant transport processes of the injected charge by adopting, as the charge source term, the distribution of the absorbed electrons as obtained by a Monte Carlo simulation. The image charge has been also introduced in the calculation in order to take into account the change in the dielectric constant when passing from the material to the vacuum. Selected computational results are reported to illustrate the role of the relevant parameters which control the charging effects in electron-irradiated insulators. [S0163-1829(97)04328-2]

I. INTRODUCTION

Charging phenomena in insulators, due, for example, to electron irradiation as it occurs in an Auger analysis, can be theoretically studied if the absorbed charge and its depth distribution are known. Moreover, one needs to evaluate the transport processes of the injected electrons in order to calculate the time evolution of the electric field both at the surface and along the depth of the irradiated insulator. The knowledge of the electric field is also relevant because, in order to avoid dielectric breakdown phenomena, the field cannot exceed some critical value which is of the order of 10^7 V/cm for SiO_2. The charge diffusion processes generally depend on the electric field, on sample temperature, and on electron mobility inside the insulator.

The mobility of the injected electrons is an important parameter. Another important process is the charge recombination near the surface (where the positive charge is left when secondary electrons are emitted). Indeed, when neglecting the electron mobility and the charge-recombination process, the dielectric breakdown conditions may be quickly attained in insulators. Let us illustrate this point with a specific example. For a 3-keV electron irradiation at a current density of 1 mA/cm^2 (these are usual conditions in Auger analysis), the dielectric breakdown (i.e., $\approx 10^7$ V/cm) is attained in $\sim 10^{-2}$ s. However, if the injected electrons are not simply implanted into the dielectric but allowed to diffuse towards the surface through the ordinary and electric field assisted diffusion processes, they may recombine with the positive charges left by the secondary emission phenomena near the irradiated surface, then dielectric breakdown can be avoided, as proved also experimentally.[1]

II. THEORETICAL FRAMEWORK

A. The Monte Carlo simulation

The Monte Carlo method (see, for example, Ref. 2) is a numerical procedure involving random numbers suitable for solving certain mathematical problems. This method is convenient for studying electron penetration in matter, so long as the probabilities of interactions of an individual electron with the atoms constituting the target are known. Consequently, it is possible to compute the macroscopic phenomena characteristic of the interaction processes by simulating a great number of trajectories and then taking an average. Many analytical approaches concerning particle-solid interaction have been proposed which, as opposed to the Monte Carlo procedures, are appealing descriptions because of the simplicity of the involved closed formulas. On the other hand, since the Monte Carlo method is a very powerful numerical tool, it has been frequently used to investigate electron and positron penetration in solid targets,[2–29] especially when purely analytical models and simple approaches using closed formulas are not able to give satisfactory results. The rapid evolution of the computer calculation capability has made possible, and convenient, detailed Monte Carlo simulations in which all scattering events are described. Such simulations are exact except for the statistical uncertainties and should give the same results as that obtained by solving the transport equations.[25]

1. The Monte Carlo scheme

Here we wish to describe the Monte Carlo scheme we have adopted to calculate the electron-implantation profile in SiO_2. Let us introduce spherical coordinates (r,θ,ϕ) and assume that a stream of monoenergetic electrons impinges

on a semi-infinite solid target in the $+x$ direction. The path-length distribution is assumed to follow the Poisson statistics. The step-length Δs is then given by

$$\Delta s = -\lambda_{\mathrm{el}} \ln(rnd_1), \tag{1}$$

where rnd_1 is a random number uniformly distributed in the range [0,1]. The elastic mean free path λ_{el} is calculated as

$$\lambda_{\mathrm{el}} = \frac{1}{N\sigma_{\mathrm{el}}}, \tag{2}$$

where σ_{el} is the total elastic scattering cross section and N is the number of atoms (or molecules in the case of compound materials) for a unit of volume in the solid. The energy loss ΔE along the segment of trajectory Δs is approximated by

$$\Delta E = (dE/ds)\Delta s, \tag{3}$$

where $-dE/ds$ is the stopping power. The polar scattering angle θ after an elastic collision is calculated by assuming that the probability $P(\theta)$ of elastic scattering into an angular range from 0 to θ is a random number rnd_2 uniformly distributed in the range [0,1]. The azimuthal angle ϕ can take on any value in the range $[0,2\pi]$ selected by a random number rnd_3 uniformly distributed in such a range.

Both the θ and ϕ angles are calculated relative to the last direction in which the electron was moving before the impact. The direction θ_x' in which the electron is moving after the last deflection, relative to the x direction, is given by

$$\cos\theta_x' = \cos\theta_x\cos\theta + \sin\theta_x\sin\theta\cos\phi, \tag{4}$$

where θ_x is the angle relative to the x direction before the impact. The incremov Δx along the x direction is then calculated as

$$\Delta x = \Delta s \cos\theta_x'. \tag{5}$$

The new angle θ_x' then becomes the incident angle θ_x for the next path length. In the present calculation an electron is followed into the solid target until its energy becomes lower than 100 eV.

2. Elastic scattering: high energy electrons

The screened Rutherford's cross section, based on the Wentzel model,[30] has been widely used in Monte Carlo simulations due its simplicity. However, unfortunately, it is valid only for high energy electrons [$E_0 \gtrsim 10$ keV (Ref. 19)] because it was derived from the first Born approximation. In this approximation and assuming that the penetrating electrons are subject to a screened Coulomb potential of the form:[30]

$$V(r) = \frac{Ze^2}{r}\exp(-\alpha r), \tag{6}$$

where

$$\alpha = \frac{Z^{1/3}}{a_0}, \tag{7}$$

and $a_0 = \hbar^2/me^2$ is the Bohr radius of hydrogen, the differential elastic scattering cross section can be given in the following closed form:

$$\frac{d\sigma(\theta)}{d\theta} = K_n \frac{Z^2}{E^2} \frac{\sin\theta}{(1-\cos\theta+2\beta)^2}, \tag{8}$$

where

$$\beta = k\frac{Z^{2/3}}{E}, \tag{9}$$

θ is the scattering angle ($d\Omega = 2\pi\sin\theta d\theta$), $K_n = (\pi e^4/2)$, and $k = (e^2/8a_0)$.

The total cross section, in such a case, is given by

$$\sigma_{\mathrm{el}} = 2\pi\int_0^{\pi}\frac{d\sigma}{d\Omega}\sin\theta d\theta = \frac{K_n Z^2}{2\beta(1+\beta)E^2}, \tag{10}$$

while the probability $P(\theta)$ of elastic scattering into an angular range from 0 to θ can be calculated as

$$P(\theta) = \frac{2\pi\int_0^{\theta}\frac{d\sigma}{d\Omega}\sin\theta d\theta}{\sigma_{el}} = \frac{(1+\beta)(1-\cos\theta)}{(1+2\beta-\cos\theta)}. \tag{11}$$

3. Elastic scattering: low energy electrons

For an electron primary energy higher than 10 keV, the screened Rutherford formula [Eq. (8)] has been frequently used.[7,17,19,20] It can be rewritten as

$$\frac{d\sigma(\theta)}{d\theta} = f(Z,E)\frac{\sin\theta}{(1-\cos\theta+\Upsilon)^2}, \tag{12}$$

where [see Eqs. (8) and (9)]

$$f(Z,E) = \frac{\pi e^4}{2}\frac{Z^2}{E^2}, \tag{13}$$

and

$$\Upsilon = 2\beta = \frac{e^2}{4a_0}\frac{Z^{2/3}}{E}. \tag{14}$$

This analytical form is very convenient because it permits us to sample the scattering angle by using the following simple closed formula:

$$\cos\theta = 1 - \frac{2P(\theta)\Upsilon}{2+\Upsilon-2P(\theta)}. \tag{15}$$

For this reason it can be convenient to use the functional form of Eq. (12) in order to approximate the differential elastic scattering cross section even when the energies of the electrons are low. In this case $f(Z,E)$ and Υ must be determined, of course, in order to accurately fit the cross sections of low energy electrons numerically computed by the partial wave expansion method. $f(Z,E)$ and Υ, in other words, must be computed so that the total elastic scattering cross section σ_{el} and the transport elastic scattering cross section σ_{tr} as-

sume the values calculated by the partial wave expansion method described in the previous paper[31] (see, for example, Baró *et al.* [24,25]).

Since

$$\sigma_{\mathrm{el}}=\int_0^{\pi}\frac{d\sigma}{d\theta}d\theta=f(Z,E)\frac{2}{\Upsilon(2+\Upsilon)}, \tag{16}$$

then

$$\frac{d\sigma}{d\Omega}=\frac{\sigma_{\mathrm{el}}}{4\pi}\frac{\Upsilon(\Upsilon+2)}{(1-\cos\theta+\Upsilon)^2}. \tag{17}$$

By definition and using the last equation we get, on the other hand,

$$\sigma_{\mathrm{tr}}=\sigma_{\mathrm{el}}\left[\frac{\Upsilon(\Upsilon+2)}{2}\ln\frac{\Upsilon+2}{\Upsilon}-\Upsilon\right]. \tag{18}$$

Let us define

$$\Xi=\frac{\sigma_{\mathrm{tr}}}{\sigma_{\mathrm{el}}}=\Upsilon\left[\frac{\Upsilon+2}{2}\ln\frac{\Upsilon+2}{\Upsilon}-1\right]. \tag{19}$$

Once the values of σ_{tr} and of σ_{el} numerically calculated are known, they can be used to obtain Ξ and hence, by mean of a bisection algorithm, the values of Υ as a function of the electron energy. The sampling of the scattering angle θ can thus be performed by inserting in Eq. (15) the value of Υ corresponding to the energy that the electron had before the elastic collision and, for $P(\theta)$, a random number uniformly distributed in the range [0,1]. For each step along each electron path, the electron energy is different: then the value of Υ has to be computed by cubic spline interpolation of a set of tabulated values of Υ previously calculated and stored.

B. Transport equation

Starting from a realistic distribution of the injected electrons in an insulator, as obtained by the above illustrated Monte Carlo simulation, it is possible to calculate the surface electric field of the electron-irradiated solid by using the Gauss law and including image-charge effects.

Since, typically, the electron-beam size, utilized, for example, in Auger analysis, is much larger than the other important lengths, namely, the maximum electron-penetration range and migration depth, it is reasonable to consider the continuity equation for the ordinary and electric field assisted diffusion process for the injected electrons in the following one-dimensional form:

$$\frac{\partial q(x,t)}{\partial t}=\frac{\mu_e k_B T}{e}\frac{\partial^2 q(x,t)}{\partial x^2}-\mu_e\frac{\partial}{\partial x}[F(x,t)q(x,t)]+S(x,t), \tag{20}$$

where $q(x,t)$ is the electron charge density at time t and depth x ($x=0$ is the surface position), k_B the Boltzmann constant, e the electron charge, T the temperature, and μ_e the electron mobility connected to the electron diffusion coefficient through the Nernst-Einstein equation. $F(x,t)$ is the electric field induced by the primary electrons as well as by the surface positive charge left by the secondary-electron emission. $F(x,t)$ may be calculated by integrating Poissons's equation:

$$\frac{\partial F(x,t)}{\partial x}=\frac{q(x,t)}{\epsilon_0\epsilon_r}, \tag{21}$$

where ϵ_0 is the vacuum permittivity and ϵ_r the dielectric constant, the value of which, for a typical glass, is 5 (for example, $\epsilon_r=4.6$ for α quartz.[32])

In the right-hand side of the continuity Eq. (20) one may recognize three contributions to the space-charge evolution as function of time:[33] the first term is simply related to the ordinary diffusion process (with a charge-concentration independent diffusion coefficient) as given by the first Fick's law; the second term is related to the drift velocity, of the charged particles, triggered by the electric field, and finally $S(x,t)$ is the deposition function of the injected electrons to be computed with the Monte Carlo method as described in the previous section.

Finally, to account for the injected-electron recombination process at the surface, where positive charges are generated when secondary electrons are emitted, the appropriate boundary condition is

$$\mu_e F(x,t)q(x,t)-\frac{\mu_e k_B T}{e}\frac{\partial q(x,t)}{\partial x}=hq(x,t), \tag{22}$$

at $x=0$.

Such a condition is used whenever a recombination process characterized by a rate proportional to h is at work,[33,34] in a system where both a diffusion and a drift current exist (instantaneous recombination). In the actual calculations this corresponds to values $h\gtrsim 1.5$ cm/s. Equations (13)–(15) describe the time evolution of the global charge density when the positive charges are immobile. The charged holes, created by bond breaking during electron irradiation, are also considered immobile. The electric field is calculated at $x=0$ at any time by using the Gauss law. We have in addition the obvious condition

$$\lim_{x\to\infty}q(x,t)=0, \tag{23}$$

for $t\geqslant 0$.

The image charge has been also introduced in the calculation in order to take into account the change in the dielectric constant when passing from the dielectric to the vacuum. The introduction of such an image charge is a standard mathematical procedure to take into account that only a portion (half) of space is occupied by the insulating material; the related boundary condition can then be treated as if an image of the actual charge is created in the vacuum. The vaule of the image charge will depend on the dielectric constant of the insulating material. Then, at any time, the electric field is obtained as the sum of the electric field created by the actual charge distribution $q(x,t)$ and by its image $Kq(x,t)$ placed in the vacuum, the plane of symmetry being $x=0$. Here K represents the image weight and is given by[35]

$$K=\frac{\epsilon_r-1}{\epsilon_r+1}. \tag{24}$$

C. The surface positive charge in electron-irradiated insulators

When an electron stream is bombarding a solid target, secondary electrons are emitted from a surface layer. The thickness of this layer, which becomes positively charged in the case of electron-irradiation of insulators, is of the order of 5–30 Å (i.e., a thickness comparable to the inelastic mean free path of an electron traveling into a solid).[36,37]

The primary electrons, on the other hand, after a number of elastic and inelastic collisions with the atoms of the target, are trapped in the material, apart from a fraction of them which come back and emerge from the surface. Since we are considering a bulk, the sum of the fractions of trapped and backscattered electrons is equal to 1.

The penetration depth of the absorbed electrons depends on the material and on the energy of the primary electrons; in general, this depth is much more greater than the thickness of the layer positively charged, at the top of the surface, produced by secondary-electron emission. For 3-keV electrons impinging on SiO_2, for instance, the penetration depth of the primary electrons is $\approx$1500 Å. For these reasons, the charge-recombination process was described as a boundary condition, at $x=0$, in Eq. (22).

Since the total stored charges, namely, the positive charge at the surface and the negative charge inside the bulk are of the same order of magnitude (and in the case of low energy electrons impinging on SiO_2 they must be practically equal, since dielectric breakdown conditions are not attained[1]) the positive charge density near the surface must be much greater than the negative charge density trapped into the solid. Concerning the nature of the surface positive charges, these are most probably trapped holes generated by the electron-collisional events which may also induce Auger electron emission.

III. RESULTS AND DISCUSSION

A. Monte Carlo calculation of the backscattering coefficient

Figure 1 shows the experimental data of Reimer and Tollkamp[38] and of Böngeler *et al.*[39] concerning the backscattering coefficient of electrons, impinging on Al, with kinetic energy ranging from 500 to 10 000 eV. The results of our Monte Carlo calculations, performed along the lines described in Sec. II, and considering two different stopping powers[40,41] are also reported. The Monte Carlo results agree quite well with the experimental data, when the primary energy is higher than $\approx$1 keV. Furthermore, for energies higher than 1 keV, the Monte Carlo results are clearly independent of the adopted stopping power. In fact, the various stopping powers are similar when the electron energy is higher than $\approx$500 eV.[31] On the other hand, when the energy is lower than 1 keV some departure from the experimental data is observed. This departure becomes particularly evident at 500 eV.

More precisely, the experimental data are lower than the values predicted by all the Monte Carlo simulations. We believe that both the approximations introduced in our calculations and the uncertainty in the backscattering measurements, possibly due to the contamination of the surfaces, can explain the slight discrepancy between theory and experiment.

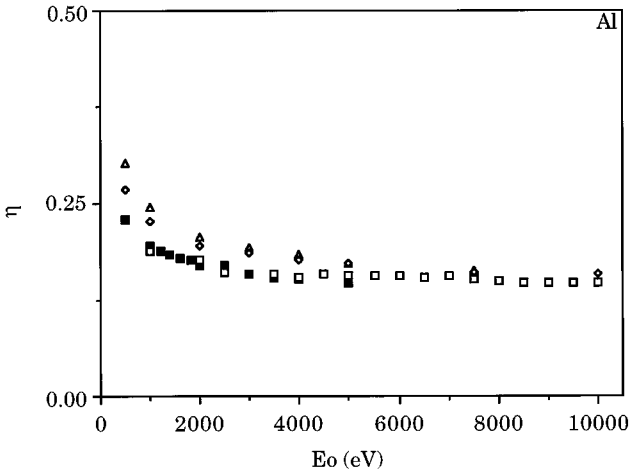

FIG. 1. Backscattering coefficient of electrons impinging on Al. Empty squares: Reimer and Tollkamp (Ref. 38) experimental data. Filled squares: Böngeler *et al.* (Ref. 39) experimental data. Triangles: Present Monte Carlo results using the Ashley and Anderson (Ref. 40) stopping power. Rhombs: Present Monte Carlo results using Joy and Luo (Ref. 41) stopping power.

The backscattering coefficient, as computed by the Monte Carlo simulation as a function of the primary energy for electron impinging on SiO_2 is compared in Table I, with the Vicanek and Urbassek formula given by[42]

$$\eta=\left(1+a_1\frac{\mu_0}{\nu^{1/2}}+a_2\frac{\mu_0^2}{\nu}+a_3\frac{\mu_0^3}{\nu^{3/2}}+a_4\frac{\mu_0^4}{\nu^2}\right)^{-1/2}, \quad (25)$$

where μ_0 ($=1$ in the present case) is the cosine of the angle of incidence, $a_1\simeq3.39$, $a_2\simeq8.59$, $a_3\simeq4.16$, $a_4\simeq135.9$, and ν is the ratio between the maximum range R and the transport mean free path $\lambda_{tr}=1/N\sigma_{tr}$. The adopted stopping power was that of Ashley and Anderson.[40]

B. Monte Carlo calculation of the electron-implantation profile

Selected examples of the electron-implantation profiles, in SiO_2, as obtained with the above illustrated Monte Carlo procedure, are reported in Fig. 2. In particular, the dependence of the electron-implantation profiles on the electron energy is illustrated when the Ashley and Anderson stopping power[40] is adopted in the Monte Carlo scheme.

Starting from these electron depth-deposition functions, the surface electric field and potential can be calculated by numerical integration of the relevant continuity equation (20), and the boundary conditions (21)–(22), for the ordinary

TABLE I. Backscattering coefficient of electrons impinging on SiO_2.

E_0 (eV)	Monte Carlo simulation	Theory of Vicanek and Urbassek (Ref. 42)
3000	0.163	0.149
5000	0.150	0.143
10000	0.139	0.137

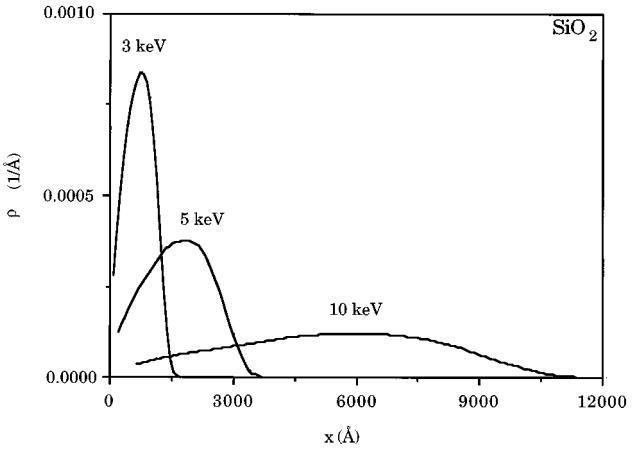

FIG. 2. Implantation profiles of electrons in SiO_2. Present Monte Carlo results using the Ashley and Anderson (Ref. 40) stopping power.

and electric-field assisted diffusion process. The main results are reported in the following section.

C. Surface electric field calculation

In Fig. 3, the numerical results for the time dependence of the surface electric field are reported. The calculations, [Eqs. (20)–(22)], are related to a primary-electron current density of 10^{-3} A/cm^2 and a 3-keV electron energy. Moreover, since the diffusion coefficient of the injected electrons in SiO_2 is not known, we have chosen to consider three values for it (10^{-6}, 10^{-7}, and 10^{-8} cm^2/s, respectively), while maintaining a fixed target temperature of 300 K. With these choices, the three curves were obtained. They clearly indicate the relevance of the diffusion coefficient parameter in determining the steady-state value of the surface electric field as well as the interval time necessary to attain stationary conditions. In Fig. 4 we presented the surface electric field for a diffusion coefficient of 10^{-6} cm^2/s and at primary energies of 3 and 5 keV: note that the energy of the primary electrons modifies the steady-state value of the electric field.

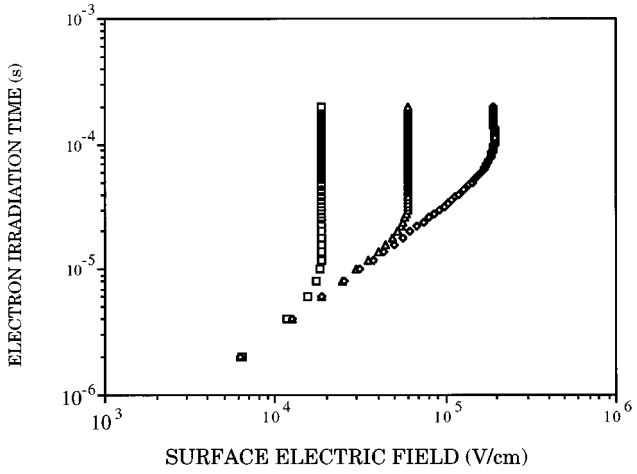

FIG. 3. Surface electric field as a function of the electron-irradiation time. Electron energy: 3 keV. Current density: 10^{-3} A/cm^2. $\delta = 1 - \eta$. Diffusion coefficient: 10^{-6} cm^2/s (squares); 10^{-7} cm^2/s (triangles); 10^{-8} cm^2/s (rhombs).

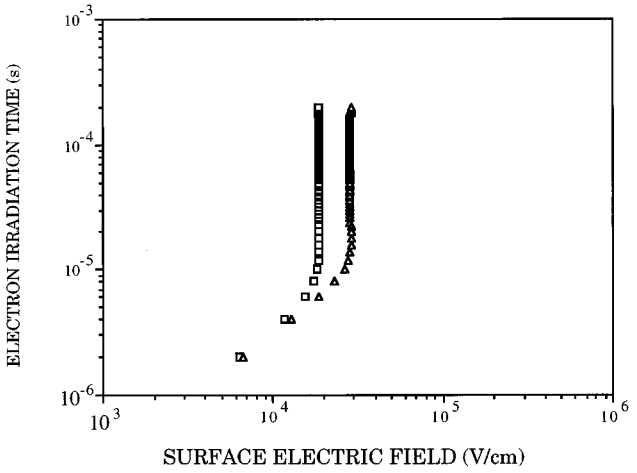

FIG. 4. Surface electric field as a function of the electron-irradiation time. Diffusion coefficient: 10^{-6} cm^2/s. Current density: 10^{-3} A/cm^2. $\delta=1-\eta$. Electron energy: 3 keV (squares); 5 keV (triangles).

Now, coming back to the relevance of the diffusion coefficient, note that a higher value of this parameter implies a more efficient charge-recombination process at the surface, along with a reduction of the unbalanced charge density and a lower value of the electric field. In the limit of a zero value of the electron mobility, a linear increasing of the surface electric field is easily anticipated with dielectric breakdown conditions attained in a very short interval time of irradiation, as discussed in the introduction. This is, on the other hand, not the case: breakdown conditions are not observed in electron irradiation of SiO_2, in typical Auger analysis conditions, and we explain such an experimental fact by looking at the electron mobility and surface recombination processes. The electron mobility alone, indeed, cannot explain stationary conditions; it is necessary that the mobile electrons recombine with the positive charges that are present near to the irradiated surface.

An additional important point related to Fig. 3 is the interval time necessary to attain steady-state conditions: this is dependent on the electron-diffusion coefficient but remains, in any case, confined to an interval time less than 10^{-4} s, i.e., negligible on the time scale typical, for example, of Auger analysis (minutes).

At this point, one may ask if the chosen values of the diffusion coefficients may have some physical basis, or, on the contrary, they are completely arbitrary. To give an answer, we note that the computed electric fields of Figs. 3, 4 correspond to values of the surface electric potentials of some electronvolts: similar values are typically observed in the shift of Auger lines, in the electron spectra, when associated to charging phenomena.[1] In addition, it is known that the stability of the Auger lines, against charging phenomena, is generally attained in a short time. The secondary emission coefficient, δ, was set, in the present calculations (Figs. 3,4), to be equal to $1-\eta$, η being the backscattering coefficient of electrons impinging on SiO_2.

In Fig. 5 we present computational results obtained with $\delta<1-\eta$ ($\delta=0.5$) and $\delta>1-\eta$ ($\delta=1.0$) as compared to results for $\delta=1-\eta$ ($\delta=0.837$). The stationary conditions are reached only when $\delta=1-\eta$, while in the other cases the

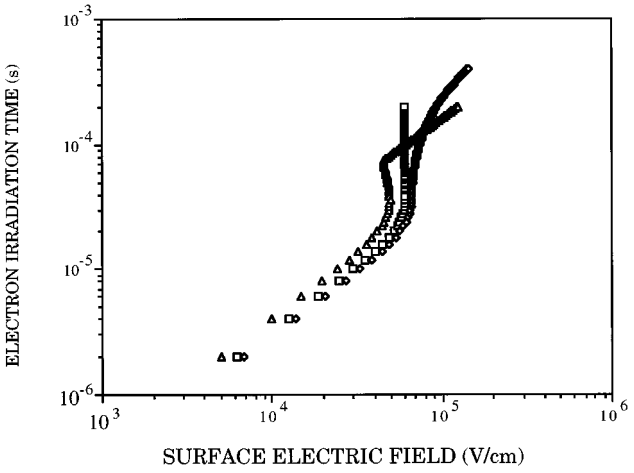

FIG. 5. Surface electric field as a function of the electron-irradiation time. Electron energy: 3 keV (squares). Current density: 10^{-3} A/cm^2. Diffusion coefficient: 10^{-7} cm^2/s. $\delta = 1-\eta = 0.837$ (squares); $\delta = 0.5$ (triangles); $\delta = 1$ (rhombs).

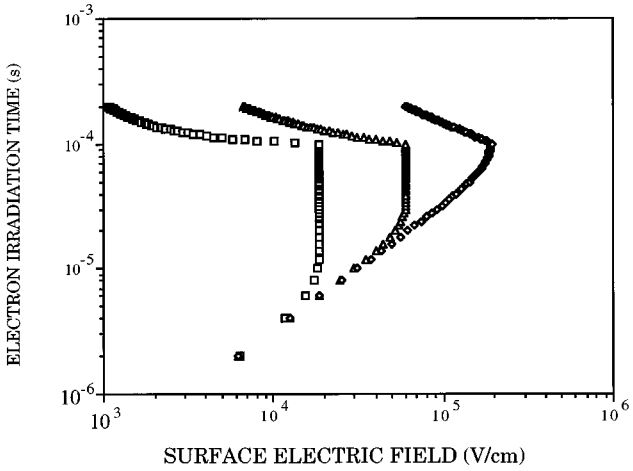

FIG. 6. Surface electric field as a function of the electron-irradiation time. Electron energy: 3 keV. Current density: 10^{-3} A/cm^2. $\delta=1-\eta$. Diffusion coefficient: 10^{-6} cm^2/s (squares); 10^{-7} cm^2/s (triangles); 10^{-8} cm^2/s (rhombs). The irradiation has been supposed to be switched off after 10^{-4} s of irradiation.

time evolution of the surface electric field exhibits an initially more complicate structure, with respect to that of Figs. 3,4, after which the field begins to increase, again towards dielectric breakdown conditions.

By swiching off the electron source, we expect that the surface electric field should decrease, due to the charge-recombination process; this is indeed demonstrated in Fig. 6 where the irradiation has been supposed to be swiched off, 10^{-4} s after the initial stage of irradiation.

IV. CONCLUSION

The time evolution of the surface electric field in an electron-irradiated insulator (SiO_2 in the present case) has been calculated by using a depth distribution of the initially trapped electrons as obtained by a Monte Carlo simulation. It is shown that steady-state values of the electric fields are attained very quickly. Their steady value depends on the electron mobility. The mobility of primary electrons and the electron-hole recombination processes at the surface of the irradiated insulators explain why the Auger technique may be applied to dielectric solids without inducing dielectric breakdown. On the other hand, the values of the electron mobility may be calculated starting from the shifts in the Auger lines, when these are associated to charging phenomena.

[1] A. Miotello, Phys. Lett. **103A**, 279 (1984).
[2] I.M. Sobol, *The Monte Carlo Method* (MIR, Moscow, 1975), pp. 38–62.
[3] H.E. Bishop, Br. J. Appl. Phys. **18**, 703 (1967).
[4] K. Murata, J. Appl. Phys. **45**, 4110 (1974).
[5] J. P. Ganachaud and M. Cailler, Surf. Sci. **83**, 498 (1979).
[6] A. Desalvo, A. Parisini, and R. Rosa, J. Phys. D **17**, 2455 (1984).
[7] F. Salvat and J. Parellada, J. Phys. D **17**, 185 (1984); **17**, 1545 (1984).
[8] S. Valkealahti and R. M. Nieminen, Appl. Phys. A **35**, 51 (1984).
[9] D. C. Joy, J. Microsc. **147**, 51 (1987).
[10] S. Ichimura, R. Shimizu, and Ding Ze-Jun, Surf. Interface Anal. **13**, 149 (1988).
[11] M. Kotera, J. Appl. Phys. **65**, 3991 (1989).
[12] A. Jablonski, Surf. Interface Anal. **14** 659 (1989).
[13] Z. Czyzewski and D. C. Joy, J. Microsc. **156**, 285 (1989).
[14] R. Browning, T. Eimori, E. P. Traut, B. Chui, and R. F. W. Pease, J. Vac. Sci. Technol. B **9**, 3578 (1991).
[15] M. M. El Gomati, W. C. C. Ross, and J. A. D. Matthew, Surf. Interface Anal. **17**, 183 (1991).
[16] G. R. Massoumi, N. Hozhabri, W. N. Lennard, and P. J. Schulz, Phys. Rev. B **44**, 3486 (1991).
[17] R. Shimizu and Ding Ze-Jun, Rep. Prog. Phys. **55**, 487 (1992).
[18] A. Akkerman, A. Gibrekhterman, A. Breskin, and R. Chechik, J. Appl. Phys. **72**, 5429 (1992).
[19] M. Dapor, Phys. Rev. B **46**, 618 (1992).
[20] M. Dapor, Appl. Surf. Sci. **70/71**, 327 (1993).
[21] R. Browning, T. Z. Li, B. Chui, Jun Ye, R. F. W. Pease, Z. Czyzewski, and D. C. Joy, J. Appl. Phys. **76**, 2016 (1994).
[22] K. Nishimura, T. Itotani, and K. Ohya, Jpn. J. Appl. Phys. 1 **33**, 4727 (1994).
[23] K. Ohya, Jpn. J. Appl. Phys. 1 **33**, 4735 (1994).
[24] J. Baró, J. Sempau, J. M. Fernández-Varea, and F. Salvat, Nucl. Instrum. Methods Phys. Res. B **84**, 465 (1994).
[25] J. Baró, J. Sempau, J. M. Fernández-Varea, and F. Salvat, Nucl. Instrum. Methods Phys. Res. B **100**, 31 (1995).
[26] K. Murata, M. Yasuda, and H. Kawata, Scanning **17**, 228 (1995).
[27] V. J. Ghosh and G. C. Aers, Phys. Rev. B **51**, 45 (1995).
[28] C. L. Lee, K. Y. Kong, H. Gong, and C. K. Ong, Surf. Interface Anal. **24**, 15 (1996).
[29] M. Dapor and A. Miotello, Scanning Microsc. **10**, No. 4 (1996).
[30] G. Wentzel, Z. Phys. **40**, 590 (1927).
[31] M. Dapor and A. Miotello, preceeding paper, Phys. Rev. B **56**, 2234 (1997).

[32] H. Chen, H. Gong, and C. K. Ong, J. Appl. Phys. **78**, 3714 (1995).
[33] H.S. Carslaw and J.C. Jaeger, *Conduction of Heat in Solids* (Clarendon, Oxford, 1959), Chap. 18.
[34] D. P. Kennedy, IEEE Trans. Electron Devices **9**, 174 (1962).
[35] J. Cazaux, J. Appl. Phys. **59**, 1418 (1986).
[36] L.C. Feldman and J.W. Mayer, *Fundamentals of Surface and Thin Film Analysis* (North-Holland, New York, 1986), pp. 125–153.
[37] A. Melchinger and S. Hofmann, J. Appl. Phys. **78**, 6224 (1995).
[38] L. Reimer and C. Tollkamp, Scanning **3**, 35 (1980).
[39] R. Böngeler, U. Golla, M. Kässens, L. Reimer, R. Senkel, and M. Sprank, Scanning **15**, 1 (1993).
[40] J. C. Ashley and V. E. Anderson, IEEE Trans. Nucl. Sci. **10**, 349 (1981).
[41] D. C. Joy and S. Luo, Scanning **11**, 176 (1989).
[42] M. Vicanek and H. M. Urbassek, Phys. Rev. B **44**, 7234 (1991).